2009 IEEE International Conference on Robotics and Automation
Kobe International Conference Center
Kobe, Japan, May 12-17, 2009

Skillful Manipulation Based on High-speed Sensory-Motor Fusion

Taku Senoo, Yuji Yamakawa, Satoru Mizusawa, Akio Namiki, Masatoshi Ishikawa and Makoto Shimojo

***Abstract*— This video introduces the demonstration of skillful manipulation using a high-speed robot system. The system consists of visual and tactile sensors at a rate of 1 kHz and a high-speed hand-arm manipulator. The high-speed sensory-motor fusion improves not just the speed of existing robot manipulations, but robotic skills by introducing the features peculiar to high-speed motion. Based on such a concept, new variations of skillful manipulation were achieved.**

I. INTRODUCTION

In recent years, many robotic manipulation systems have been developed. However such systems were designed with a primary goal of the emulation of human capabilities, and less attention to pursuing of the upper limit in terms of speed for mechanical systems.

To achieve such dynamic fast motion, we have developed a high-speed manipulation system. This system consists of a multi-fingered hand with tactile sensors, a wire-drive arm, and a stereo active vision system. The cycle time of sensor feedback and control processing is set at 1ms. Therefore the robot can react quickly to target motion in unpredictable conditions.

Moreover new strategies for high-speed manipulation are developed utilizing the feature of high-speed motion. Several tasks show that high-speed active control enables stable and robust manipulation. In addition such a high-speed control strategy can be applied to various complicated manipulation. This result indicates that high-speed manipulation improves robotic skills.

II. SYSTEM CONFIGURATION

A. Motor System

The hand [1] consists of three fingers and a wrist. It has 10-DOF in total. A small harmonic drive gear and a high-power mini actuator are fitted in each finger link. The design of this actuator is based on the new concept that maximum power output, rather than rated power output, should be improved. The hand can close its joints at 180 [deg] per 0.1 [s]. Its maximum velocity is 300 [rpm], and the maximum output is 12 [N].

The arm is a wire-drive manipulator (Barrett Technology Inc.). The manipulator has 4-DOF consisting of alternately revolution and bending motion. High-speed movement with maximum velocity of the end-effector of 6 [m/s] and maximum acceleration of 58 [m/s^2] is achieved.

The hand-arm system is shown in Fig.1 (a).

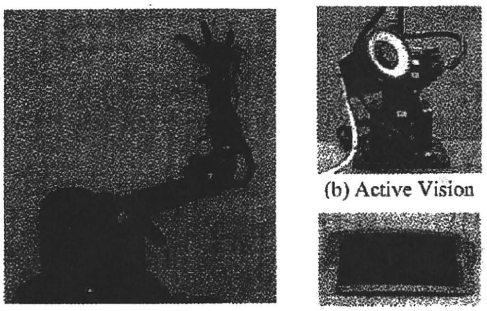

(a) Hand-Arm System (b) Active Vision (c) Tactile Sensor

Fig. 1. System configuration

B. Sensory System

Figure 1 (b) shows a column parallel vision system (CPV) [2] mounted on the 2-DOF (tilt and pan) active mechanism. The CPV has 128×128 pixel photo detectors and an all pixel parallel processing array. Various visual processing (moment detection, segmentation and so on) are achieved within 1 ms because execution is in parallel.

The tactile sensor [3] is a sheet-like object as shown in Fig.1 (c). The sensor consists of the two outer electrically conductive films and the inner pressure-conductive rubber. The sensor can measure the center position of a two dimensional distributed load and the total load within 1 ms. The sensor is attached to the top link of each finger.

III. SKILLFUL MANIPULATION

A. High-speed Manipulation

A high-speed robot system improves not just the speed of existing robot manipulations. Pursuing the upper limit in terms of manipulation speed, we have developed appropriate new control for high-speed manipulation. Here stable and robust manipulation by introducing the features peculiar to high-speed motion are presented as shown in Fig.2.

1) Dribbling: The hand dribbles a small ball between two fingers [4]. The dribbling period is around 100 ms. In this task, new concept called "dynamic holding" is proposed. This means that high-speed active control enables the maintaining of periodically stable motion. Through dynamic holding states, there is an increasing possibility that novel transition of contact state is achieved.

T. Senoo, Y. Yamakawa, S. Mizusawa and M. Ishikawa are with Dept. of Creative Informatics, Graduate School of Information Science and Technology, University of Tokyo, 7-3-1 Hongo, Bunkyo-ku, Tokyo 113-8656, Japan. Taku_Seno@ipc.i.u-tokyo.ac.jp

A. Namiki is with Dept. of Mechanical Engineering, Graduate School of Engineering, Chiba University, 1-33 Yayoi-cho Inage-ku Chiba-shi, Chiba 263-8522, Japan. namiki@faculty.chiba-u.jp

M. Shimojo is with the Dept. of Mechanical Engineering and Intelligent Systems, Univ. of Electro-Communications, 1-5-1 Chofugaoka, Chofu-shi, Tokyo 182-8585, Japan. shimojo@mce.uec.ac.jp

978-1-4244-2789-5/09/$25.00 ©2009 IEEE

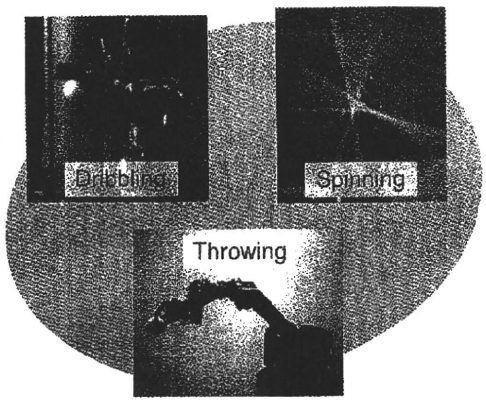

Fig. 2. High-speed manipulation

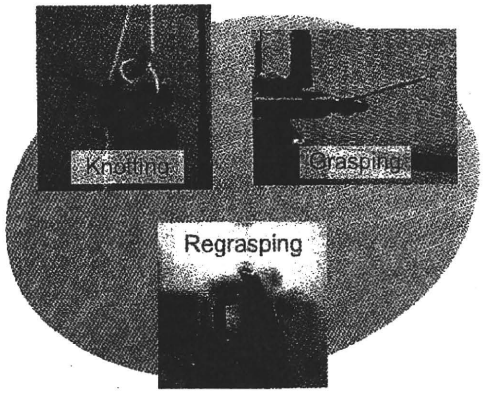

Fig. 3. Complicated manipulation

2) Pen Spinning: The hand repeats alternately the rotation of a pen-shaped object using left and center fingers and using right and center fingers [5]. The spinning strategy is based on the feature that rotational motion is stable when its speed is fast. Moreover the contact force and the timing of shifts about the axis of rotation are controlled in real-time by tactile feedback.

3) Throwing: The hand-arm manipulator throws a ball towards the target [6]. The release control with three fingers is designed so that the error of the ball direction is reduced using the apparent force, which is generated by high-speed arm swing. In order to achieve high-speed arm swing a kinetic chain algorithm is also presented, which is a mechanism to explosively radiate kinetic energy.

B. Complicated Manipulation

Such new control strategies for high-speed manipulation can be expanded to more complicated manipulations. We achieved skillful handling of more practical objects as shown in Fig.3.

1) Knotting of a Rope: Manipulation of flexible objects with robotic hands is a difficult issue. We have challenged to knot a rope as a simple example [7]. By high-speed sensory feedback control, the hand can dexterously control a flexible object regardless of its unpredictable moiton. Moreover a new strategy of motion for robot hands corresponding to mathematical elements of knot theory is presented.

2) Grasping with Tweezers: Considering robots work in human society, it is important for robot hands to handle a typical human tool. We achieved grasping a rice grain and a screw with tweezers [8]. High-speed visual servoing enables the control of force between a finger and a tool in real-time. This result means that a robot hand can handle many objects of various sizes with a tool.

3) Dynamic Regrasping: A new type of regrasping using high-speed performance is developed [9]. The dynamic regrasping consists of throwing and catching unlike with previous one while keeping a contact state. We achieved dynamic regrasping for objects of which mass distribution is not uniform and different-shaped objects.

IV. CONCLUSIONS

These videos show that high-speed sensory-motor fusion has great potential to produce new control strategies and new robotic skills. Integrating high-speed dynamic manipulation as shown in this video and conventional static manipulation, more suitable robotic work for practical use would be realized.

These experimental results and other manipulations are shown on the web site [10].

REFERENCES

[1] A. Namiki and Y. Imai and M. Ishikawa and M. Kaneko, *Development of a High-speed Multifingered Hand System and Its Application to Catching*, IEEE/RSJ Proc. of Int. Conf. on Intelligent Robots and Systems, pp.2666-2671, 2003.

[2] Y. Nakabo, M. Ishikawa, H. Toyoda and S. Mizuno, *1ms Column Parallel Vision System and It's Application of High Speed Target Tracking*, Proc. of IEEE Int. Conf. on Robotics and Automation, pp.650-655, 2000.

[3] M. Shimojo, A. Namiki, M. Ishikawa, R. Makino and K. Mabuchi, *A Tactile Sensor Sheet Using Pressure Conductive Rubber With Electrical-Wires Stitched Method*, IEEE Sensors Journal, Vol.4, No.5, pp.589-596, 2004.

[4] D. Shiokata, A. Namiki and M. Ishikawa, *Dynamic Dribbling Using a High-speed Multifingered Hand and a High-speed Vision System*, IEEE/RSJ Proc. of Int. Conf. on Intelligent Robots and Systems, pp.3945-3950, 2005.

[5] T. Ishihara, A. Namiki, M. Ishikawa and M. Shimojo, *Dynamic Pen Spinning Using a High-speed Multifingered Hand with High-speed Tactile Sensor*, IEEE/RSJ Proc. of Int. Conf. on Humanoids, pp.258-263, 2006.

[6] T. Senoo, A. Namiki and M. Ishikawa, *High-speed Throwing Motion Based on Kinetic Chain Approach*, IEEE/RSJ Proc. of Int. Conf. on Intelligent Robots and Systems, pp.3206-3211, 2008.

[7] Y. Yamakawa, A. Namiki, M. Ishikawa and M. Shimojo, *Knotting Manipulation of a Flexible Rope by a Multifingered Hand System based on Skill Synthesis*, IEEE/RSJ Proc. of Int. Conf. on Intelligent Robots and Systems, pp.2691-2696, 2008.

[8] S. Mizusawa, A. Namiki and M. Ishikawa, *Tweezers Type Tool Manipulation by a Multifingered Hand Using a High-speed Visual Servoing*, IEEE/RSJ Proc. of Int. Conf. on Intelligent Robots and Systems, pp.2709-2714, 2008.

[9] N. Furukawa, A. Namiki, T. Senoo and M. Ishikawa, *Dynamic Regrasping Using a High-speed Multifingered Hand and a High-speed Vision System*, Proc. of IEEE Int. Conf. on Robotics and Automation, pp.181-187, 2006.

[10] http://www.k2.t.u-tokyo.ac.jp/fusion/index-e.html

Paper:

High Speed and High Sensitivity Slip Sensor Utilizing Characteristics of Conductive Rubber

–Relationship Between Shear Deformation of Conductive Rubber and Resistance Change–

Seiichi Teshigawara*, Kenjiro Tadakuma*, Aiguo Ming*, Masatoshi Ishikawa, and Makoto Shimojo***

*Department of Mechanical Engineering and Intelligent Systems, The University of Electro-Communications
1-5-1 Chofugaoka, Chofu, Tokyo 182-8585, Japan
E-mail: teshigawara@rm.mce.uec.ac.jp
**Department of Mathematical Engineering and Information Physics, Faculty of Engineering, The University of Tokyo
7-3-1 Hongo, Bunkyo-ku, Tokyo 113-0033, Japan
[Received October 20, 2008; accepted January 17, 2009]

Humans can grasp an object without information such as a coefficient of friction or weight. To implement this grasping motion with the robot hand, sensors have been proposed that detect an incipient slip within the contact surface or stick-slip. A large number of slip sensors have been proposed, but small, flexible, and practical slip sensors are currently not available yet. We have been involved in research and development activities for a center of pressure (CoP) tactile sensor that is small and flexible. This sensor uses a pressure conductive rubber to detect the central position of the load distribution and total load. As a result of using the sensor to make experiments on slip detection, we found that a peculiar change appeared in the load output of the sensor immediately before the slip displacement of an object occurred. Based on this output change, we proposed a control method that was capable of setting a grasping force in accordance with the weight of an object. However, the principle was not made clear that caused the output change to occur. We hypothesized that the change was caused by the characteristics of the pressure conductive rubber used for the material of the sensor. As a result of making verification experiments based on this hypothesis, we found that the output change was due to a change in the resistance value when the pressure conductive rubber shear deformed. It was also found that the scale of a change in the resistance value was dependent largely upon the shear deformation speed of the pressure conductive rubber. This paper describes the principle that a peculiar change occurs in the CoP sensor immediately before the occurrence of an object slip. It also reports the characteristics of the pressure conductive rubber that have newly been made apparent.

Keywords: slip detection, pressure conductive rubber, tactile sensor

1. Introduction

A tactile sensor that collects information such as contact force, slip, and temperature senses is needed for a robot to take action in such a way that it works instead of the human hand. Particularly, if the robot grasps an object of which weight is unknown, puts the grasped object on the table smoothly on the table, or delivers it to someone, the slip sense plays an important role. For this reason a variety of slip sensors have been proposed.

Johansson et al. [1, 2] researched human grasping motion and clarified that humans grasped an object with the minimum grasping force causing a slip to occur. They also showed a partial slip is important between the skin and the grasped object. A partial slip is the one that occurs between an object within the contact surface and the skin surface. It is said that the slip displacement of an object is generated by the extended area of a partial slip and then its transition to the entire slip. If a partial slip is detected that occurs immediately before its transition to the entire slip, an object can be grasped with the minimum grasping force and without slipping it off. Trembley et al. [3] proposed a slip sensor detecting this partial slip at the first time. They placed two acceleration sensors in a spherical silicon rubber with projections called the "nib" to develop a sensor that detected vibration when a partial slip occurred on the surface of the sensor. Howe et al. [4] placed four PVDF films in a semi-cylindrical silicon rubber to develop a sensor that detected vibration when a partial slip occurred on the surface of the sensor. Maeno et al. [5] modeled the structure of the human finger tissue by using the infinite element method in addition to the perception of Johansson et al. to clarify the nature of an individual tactile receptor. They simulated a human grasping method to develop a sensor with strain gauges arranged within a curved elastic body at certain intervals [6, 7]. This indicated it possible to detect a partial slip and grasp an object whose weight and coefficient of friction

are unknown. Ikeda et al. [8] proposed a method to use a camera to observe the surface of contact between an elastic body and a rigid plate and presume a slip tolerance. As described above, the detection methods are different, but many research and development activities are reported for such sensors that detect a change immediately before the slip of an object, that is, an "incipient slip."

On the other hand, we propose a method that utilizes a sensor detecting the load of a tangential force generating an object to slip to increase a grasping force before a slip displacement occurs in an object and prevent it from slipping [9]. This method employs the 2-dimensional CoP sensor developed by our laboratory. We have experimentally confirmed the characteristics that if an object is slipped on the CoP sensor, the load output drops immediately before the slip displacement of the object and that if the slip displacement occurs, the load output returns to its original level. The sensor uses these characteristics to detect a change immediately before a slip occurs [10]. We have proven that this method is capable of grasping an object with a proper grasping force and almost no slip displacement even if the weight of an object is different. The method has also succeeded in grasping a cup whose weight changes on the way (**Fig. 1**).

Reference [9] does not clarify the principle that slip of an object causes a change to occur in the load output of the CoP sensor. In this paper, Section 2 briefly describes the principle of the CoP sensor and a change in the load output due to a slip. In Section 3, we use a simple configuration consisting of electrodes and a pressure conductive rubber to make an experiment that an object is slipped on the silicon rubber surface and then describes the principle that a change occurs in the load output of the CoP sensor. Section 4 discusses an experiment that investigated the characteristics of a change in the resistance value for the shear deformation of the pressure conductive rubber and that reports the characteristics of the rubber that have been made apparent.

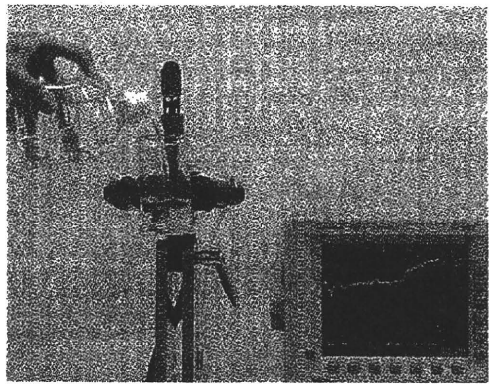

Fig. 1. Grasping force control for the object whose weight change (pouring water into a cup).

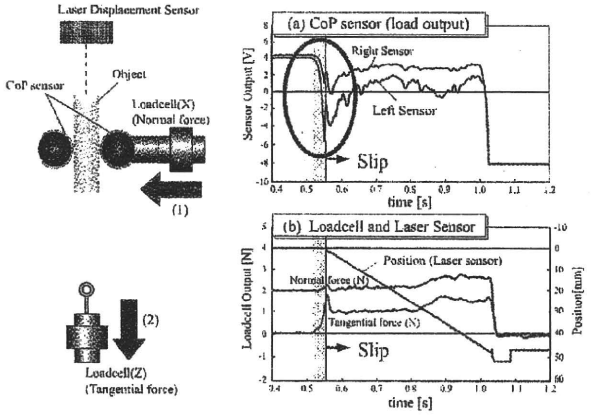

Fig. 2. Result of slip detection experiment using CoP tactile sensor.

2. Load Output Change of CoP Sensor

The CoP sensor is structured in such a way that a pressure conductive rubber (made by Inaba Rubber Co.) is sandwiched between two conductive films on layers A and B [12]. It is capable of detecting the central position of the load distribution and the total load. It is characterized mainly by flexibility, thinning, lightweight, wire saving, and high-speed responsiveness within 1 ms.

Reference [10] made an experiment that the CoP sensor was mounted on a cylinder simulating the fingertip of the robot hand to grasp an object with a certain force and slip it vertically downwards. The model of this experiment is illustrated in the left of **Fig. 2**. We measured a normal force and a tangential force (tensile force of an object) by using the load cell to compare a change in the output of the CoP sensor with the actual force working on the surface of the sensor. As a result, almost no change was found in the normal force from immediately before and after the object slipped. However, it was found that the load output of the CoP sensor significantly decreased (area graph-circled in **Fig. 2**). As the CoP sensor is a sensor to detect the load in the normal direction, such an output change cannot usually be thought to occur. On the other hand, compared with the tangential force, the timing of a decrease in the load output of the CoP sensor is coincident with that of the tangential force to act. This implies that the tangential force was added to cause some change in the sensor, resulting in such a change as above. The next section examines the cause of this output change.

3. Load Output Change in CoP Sensor and Resistance Change in Pressure Conductive Rubber

From the principle, a load output change in the CoP sensor is dependent upon a resistance change in the pressure conductive rubber. It is presumed that the deformation of the pressure conductive rubber occurring when an object slips causes its resistance to change. In the con-

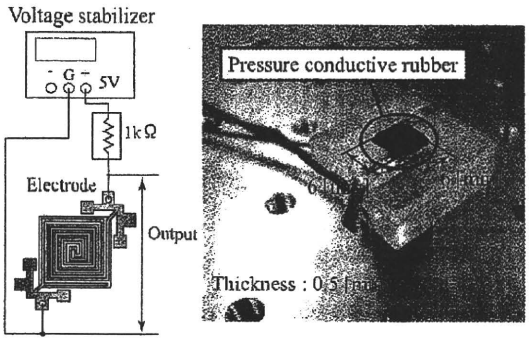

Fig. 3. Pressure conductive rubber and electrodes.

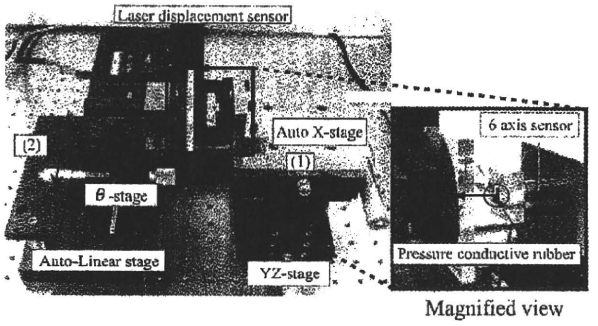

Fig. 4. Experimental equipment to generate slip.

figuration consisting of a pressure conductive rubber and electrodes excluding the arithmetic circuit of the CoP sensor, we make an experiment to observe a voltage change in between electrodes when an object is slipped on the surface of the rubber. Based on this experiment, we consider the principle of a load output change occurring in the CoP sensor that is generated immediately before the slip of an object.

3.1. Experimental Method

The configuration of the electrodes and pressure conductive rubber used for our experiment is shown in **Fig. 3**. Two electrodes are alternately spiral The pressure conductive rubber (6 mm × 6 mm) is mounted on these electrodes, which are connected through a resistance of 1 kΩ to the DC power supply. This configuration is mounted on experimental equipment in **Fig. 4**. A 6-axis sensor as shown in **Fig. 4** is placed to examine an acting force when an object is slipped on the surface of the pressure conductive rubber. An acrylic plate is place opposed to the 6-axis sensor and is pushed against the surface of the pressure conductive rubber, then slipped towards X. The 6-axis sensor is mounted to an automatic precision stage (TSD-1001SR+SOM-B25E made by Sigma Koki Co.) at the right side, which is driven towards **Fig. 4(1)**. This enables a pushing force against the acrylic plate to be automatically adjusted. On the other hand, the acrylic plate is fixed to an automatic stage (SGSP26-100 made by Sigma Koki Co.), which is driven towards **Fig. 4(2)** and can adjust its speed from 1 μm/s to 100 mm/s. As a result, the acrylic plate can be moved at a certain speed and its displacement can be measured by the laser displacement sensor (resolution: 0.1 μm) located in the recess of experimental equipment.

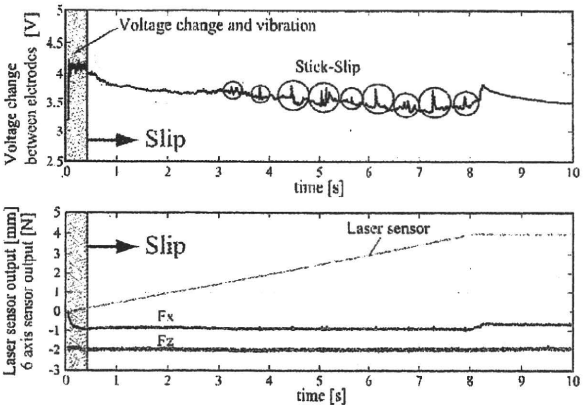

Fig. 5. Result of slip experiment.

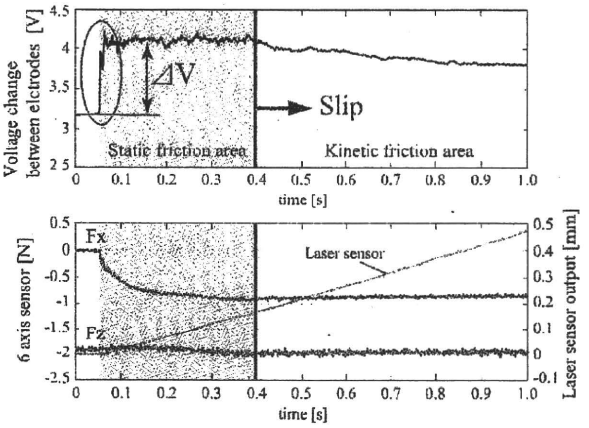

Fig. 6. Voltage change from 0 s to 1 s.

This experiment used a pushing force of about 2 N, a moving speed (slipping speed) of 0.5 mm/s, and a moving displacement of 4 mm to slip the acrylic plate on the surface of the rubber. Under this condition, we measured a potential change between electrodes and the outputs of the 6-axis sensor and laser displacement sensor.

3.2. Experimental Results

The results of this experiment are shown in **Fig. 5** and an enlarged graph between **Fig. 5**, 0 s and 1 s in **Fig. 6**. The upper graph shows a voltage change between electrodes, while the lower graph shows the outputs of the laser displacement sensor and 6-axis sensor. F_z in the lower graph is the load output of the 6-axis sensor towards Z and indicates the pushing force (normal force) of the acrylic plate. F_x is the load output of the 6-axis sensor towards X and indicates the directional force (tangential force) of slipping the acrylic plate.

The output of the 6-axis sensor in the lower part of **Fig. 5** caused normal force F_z to become almost constant (2 N) for a period from immediately before a slip occurred until it stopped. On the other hand, tangential force F_x increased up to about 0.4 s and then became constant. In other words, the section up to about 0.4 s can be considered a static friction area and subsequently a dynamic friction area. A slip on the acrylic plate and the surface of the pressure conductive rubber occurs after 0.4 s.

Looking at a voltage change in the static friction area in **Fig. 6**, the voltage rose at the same time when tangential force F_x began to be applied. A small and complicated voltage change occurred while tangential force F_x was increasing and then became almost constant. The laser displacement sensor had an output change of about 0.1 mm during this period. Looking at a voltage change in the dynamic friction area in **Fig. 5**, it was found that when the static friction area changed to the dynamic friction area, the voltage dropped and that a small change subsequently appeared at random (circled area in the upper graph).

3.3. Considerations

A voltage rose between electrodes at the same time when a tangential force was loaded on the surface of the pressure conductive rubber. This change means a decrease in the load output of the CoP sensor. It was therefore found that a peculiar load output change in the CoP sensor was caused by the characteristics of the pressure conductive rubber. If an object is slipped on the pressure conductive rubber, shear deformation is generated by the tangential force. This may cause a resistance change in the pressure conductive rubber to occur. The following paragraphs discuss the principle of generating this phenomenon. The pressure conductive rubber is the one that carbon particles are dispersed equally to a high polymer material composed mainly of a silicon rubber. Accordingly,

(1) As carbon particles contained in the rubber are separated from each other as shown in **Fig. 7(a)**, the resistance is ∞ and no current flow even if voltage is applied.

(2) As shown in **Fig. 7(b)**, the pressure conductive rubber deform in the perpendicular direction, carbon particles contained in the rubber contact each other to form a current route. At this time, resistance drops.

(3) When shear deformation as in **Fig. 7(c)** is added under the condition of **Fig. 7(b)**, the internal state of the rubber, that is, the current route is divided into some pieces and a resistance may increase at this time.

From these facts, it can be considered that a load output changes in the CoP sensor because the resistance of the pressure conductive rubber changes due to the shear deformation of the rubber occurring when an object slips on the sensor.

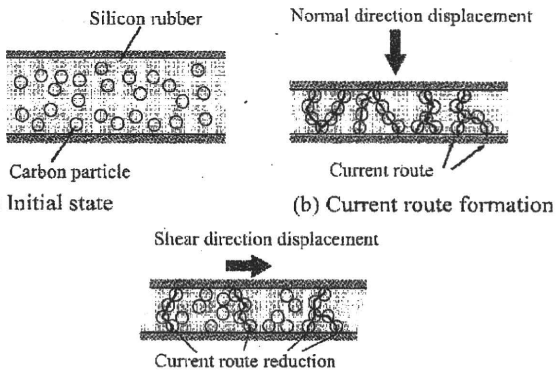

Fig. 7. Mechanism of resistance change.

Moreover, It was found that the complicated voltage change occurs at almost the same voltage immediately after a potential rose. The following causes may trigger this vibration, but they must be checked in more detail.

- Internal particles repeat separate and contact severely when shear deformation occurs.
- An partial slip occurs between the surface of the acrylic plate and the pressure conductive rubber, and the stick and slip areas change in contact area [7].

Looking at voltage changes after the acrylic plate slips, only small changes occur as the areas indicated by circles in the upper graph of **Fig. 5**. This appears in the output of tangential force F_x. It can therefore be considered that these changes are caused by the stick and slip occurring on the acrylic plate and the surface of the pressure conductive rubber.

From the above, it was found as the new characteristic of the pressure conductive rubber that a resistance was changed by shear direction deformation. It also became apparent that a complicated change occurred immediately after a resistance change was caused by shear direction deformation. The following sections pay attention to the characteristics of the former and examine what parameters a resistance change caused by the shear direction deformation relate to.

4. Shear Deformation and Resistance Change of Pressure Conductive Rubber

As described in the preceding section, the pressure conductive rubber was found to cause its resistance change to occur by shear direction deformation. In this section, we check to see what parameters this change relates to when deformation occurs or whether or not the similar output change is obtained by any shear deformation. This section pays attention to a voltage change in the static friction area based on the configuration consisting of electrodes and the pressure conductive rubber used in the preceding section and observes a voltage change if the amount

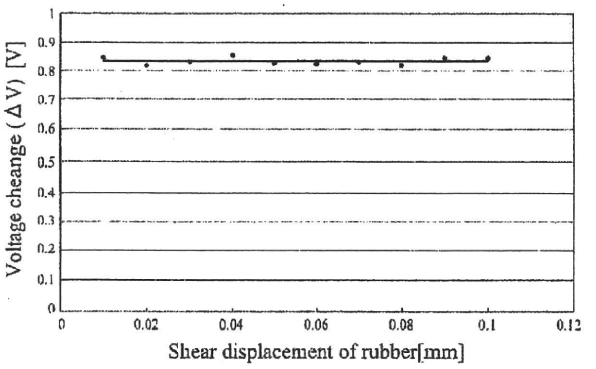

Fig. 8. Amount of shear deformation and change of voltage between the electrodes.

and speed of shear deformation and a normal force are changed.

4.1. Relation to Amount of Shear Deformation

Firstly, we examine what level of shear deformation in the pressure conductive rubber causes a resistance change to appear. This answer is already made apparent to some extent from the previous experimental results. The output results of the laser displacement sensor in **Fig. 6** have shown that the voltage reaches the maximum value in the area where the moving amount of the acrylic plate is 0.01 mm or less. If a shear deformation of 0.01 mm occurs in the pressure conductive rubber, a change may appear in the output. For checking purposes, we used the experimental equipment used in Section 3 to modify the setup of the automatic stage and carry out an experiment that changed the movement quantity of the acrylic plate.

In this experiment, we set the movement speed of the acrylic plate to 0.05 mm/s, an initial load to 1.0 N and measured amount of a voltage change ΔV when we decreased the movement quantity of the plate to 0.1 mm through 0.01 mm at intervals of 0.01 mm. The graph in **Fig. 8** sums up the amount of a voltage change (ΔV) for the amount of each shear deformation.

Data in the figure results from three measurements of the amount of each shear deformation and shows their averages. The standard deviation of the amount of each deformation was a maximum of 0.04 V. The approximation curve for this result was almost parallel to the X-axis. In spite of a decrease in the amount of rubber shear deformation from 0.1 mm to 0.01 mm, almost the same voltage change occurred. This implies that a shear deformation amount of 0.01 mm is large enough to cause a resistance change to occur in the pressure conductive rubber.

4.2. Relation to Shear Deformation Speed

The results of the preceding section have shown that a resistance change is less dependent on the amount of shear deformation. In this section, we make an experiment that changes the shear deformation speed given to the pressure conductive rubber to examine the relationship

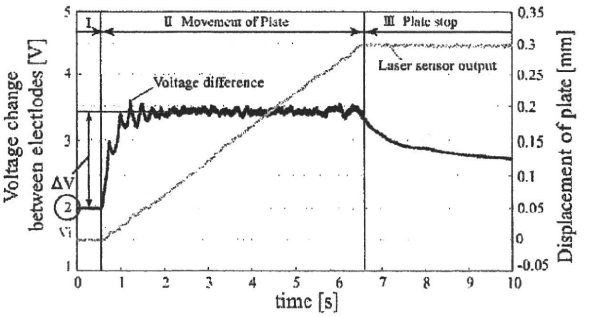

Fig. 9. Result of 0.05 mm/s.

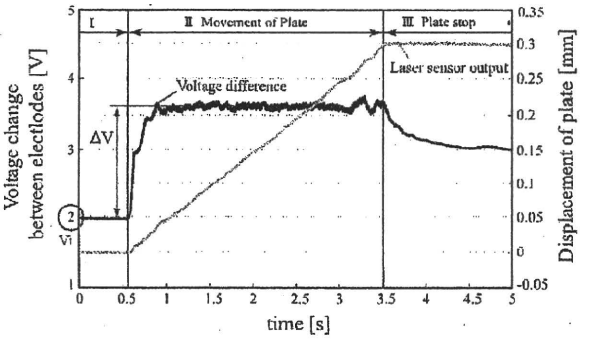

Fig. 10. Result of 0.1 mm/s.

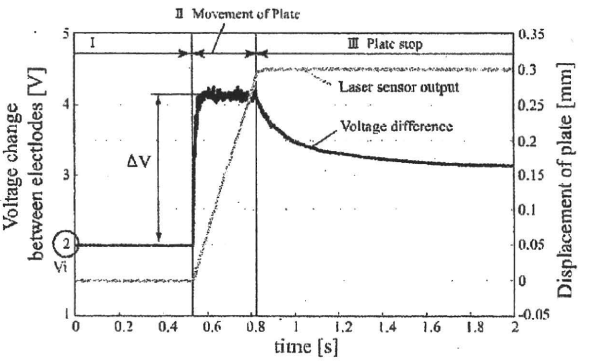

Fig. 11. Result of 1.0 mm/s.

between them. We pushed the acrylic plate against the rubber surface and applied a constant load of about 1.7 N in the normal direction and decreased a voltage between electrodes from 5 to 2 V. Under this condition, we set the movement quantity of the acrylic plate to 0.3 mm and a plate moving speed to 0.05, 0.1, and 1.0 mm/s. Then, we measured the amount of a voltage change between electrodes and the output of the laser displacement sensor.

The results of this experiment are shown in **Figs. 9**, **10**, and **11**. The vertical axis is a voltage between electrodes and the horizontal axis is time. The I area is the condition under which the acrylic plate is pushed against the pressure conductive rubber to give a normal direction distortion. The II area is the condition under which the stage is driven and the plate moves to the tangential direction. The III areas are the condition under which the plate stops. It

Table 1. Amount of voltage change between electrodes when shear deformation speed change.

Deformation speed [mm/s]	ΔV [V]
0.05	1.4
0.1	1.6
1.0	2.1

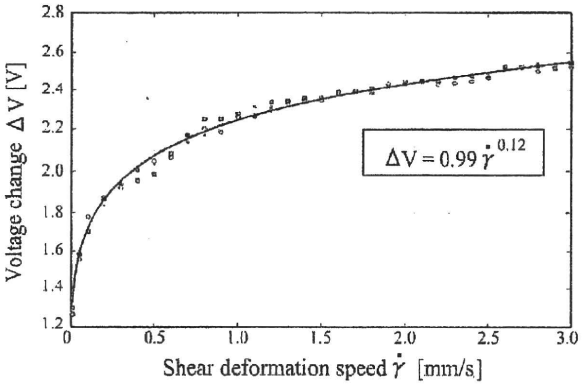

Fig. 12. Shear deformation speed of pressure conductive rubber and change of voltage between the electrodes.

was found that amount of a voltage change ΔV occurred at any shear deformation speed. **Table 1** lists a summary of a voltage change ΔV for **Figs. 9** to **11**. This table shows that ΔV changes in accordance with the shear deformation of the rubber. So, we changed this speed from 0.01 to 3.0 mm/s at proper intervals to measure ΔV.

Figure 12 shows the relationship between amount of a voltage change ΔV and the shear deformation speed. We made three measurements at each speed and plotted all pieces of data. From **Fig. 12**, it was found that the amount of a voltage change between electrodes was dependent on the shear deformation speed of the pressure conductive rubber to increase. This result has shown that the amount of a resistance change in the pressure conductive rubber by shear deformation is dependent largely on the shear deformation speed. The curve in **Fig. 12** is an approximation curve for each plot. The equation in the figure corresponds to the approximation curve found. It implies that the following relationship exists between shear deformation speed γ of the pressure conductive rubber and amount of a voltage change ΔV.

$$\Delta V = k \times \dot{\gamma}^n \quad \ldots\ldots\ldots\ldots\ldots\ldots \quad (1)$$

where coefficient k and index n are certain constants.

4.3. Effect by Normal Force

From the above, a resistance change in the pressure conductive rubber by shear deformation was found dependent on the shear deformation speed. However, the pressure conductive rubber is a material that usually causes a resistance change to occur for normal deformation. If the amount of normal deformation is changed, it has effect

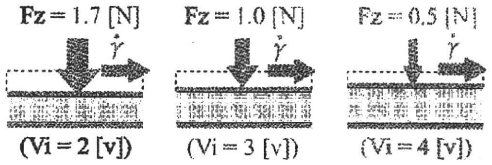

Fig. 13. The change of normal force.

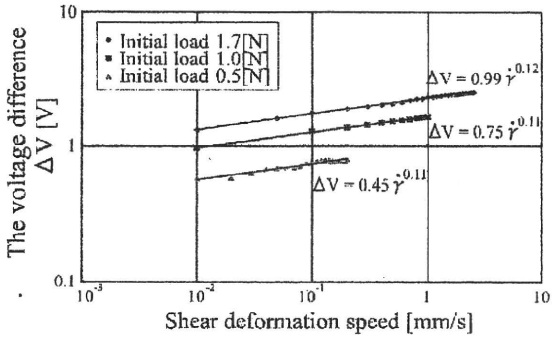

Fig. 14. Both logarithm graph.

on a resistance change by shear deformation. This section examine the relationship between shear deformation speed γ and amount of a voltage change ΔV to check its effect.

In addition to the results of the preceding section, we changed an initial load to 0.5 and 1.0 V as in **Fig. 13** to examine the relationship between γ and ΔV. When the initial load was 0.5 or 1.0 N, a voltage between electrodes was 4 or 3 V, respectively. The potential at this time is assumed an initial voltage of V_i. The data obtained from this experiment is shown in the form of the both logarithm graph in **Fig. 14**. In either case, the approximation lines in the graph show a linear increase in amount of a voltage change ΔV with an increase in shear deformation speed. These lines are almost parallel. From the approximation equation in the figure, the normal load, that is, the value of k in Eq. (1) is found to change depending on the amount of distortion. From this fact, k can be said the function of ε. Thus, Eq. (1) is as follows:

$$\Delta V = k(\varepsilon) \times \dot{\gamma}^n. \quad \ldots\ldots\ldots\ldots\ldots\ldots \quad (2)$$

A resistance change in the pressure conductive rubber was found dependent on normal distortion (ε) and shear direction distortion speed (γ).

4.4. Considerations

Like our experiments, the deformation that keeps an interval of a pair of surfaces opposed to each other and to move one of them in its surface, that is, shear deformation is not accompanied by a volume change [13]. Even if the amount of shear deformation given to the pressure conductive rubber was decreased to 0.01 mm, a resistance change remained almost unchanged in size. As considered in Section 3, a resistance change might occur due to

Table 2. Coefficient and index of approximation of **Fig. 14**.

Initial voltage (V_i)	Coefficient (k)	Index (n)
2	0.99	0.12
3	0.75	0.11
4	0.45	0.11

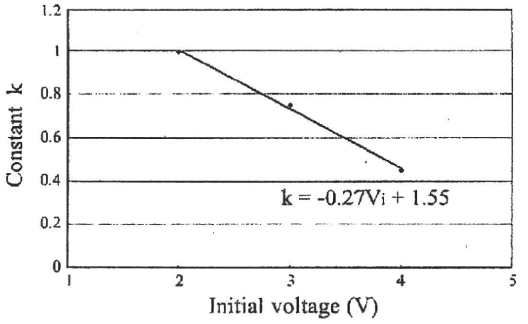

Fig. 15. Relation between coefficient (k) and initial voltage (V_i).

distributed changes in particles inside the pressure conductive rubber.

A resistance change following the shear deformation of the pressure conductive rubber was found dependent largely on shear deformation speed ($\dot{\gamma}$). In other words, in case of slow shear deformation, the internal condition of the pressure conductive rubber also slowly changes. Under this condition, the current route is resistant to be divided or even if divided, it is reformed. In case of quick shear deformation, as the internal condition of the pressure conductive rubber rapidly changes, it seems that the divided amount of the current route increased with an increase in the speed, resulting in a larger amount of resistance change.

If Eq. (2) is deformed like Eq. (3), it shows that rubber shear deformation speed ($\dot{\gamma}$) can be found by measuring normal distortion (ε) amount of a voltage change (ΔV) between electrode.

$$\dot{\gamma} = \left(\frac{\Delta V}{k(\varepsilon)}\right)^{-n} \quad \ldots\ldots\ldots\ldots\ldots \quad (3)$$

Table 2 lists a summary of k and n values from the approximation equation in **Fig. 14**. As the value of index n is almost constant, it is assumed 0.11. Voltage V_i in the table is a voltage between electrodes when normal distortion is given to the rubber. **Fig. 15** shows a graph with V_i on the horizontal axis and the value of k on the vertical axis. The graph becomes a straight line and initial voltage V_i is proportional to k. The relational equation between them is as follows:

$$k = -0.27V_i + 1.55. \quad \ldots\ldots\ldots\ldots \quad (4)$$

Together with Eq. (3), rubber shear deformation speed γ is given by the following equation:

$$\dot{\gamma} = \left(\frac{\Delta V}{-0.27V_i + 1.55}\right)^{-0.11} \quad \ldots\ldots\ldots \quad (5)$$

In other words, this equation shows that the rubber shear deformation speed can be detected by measuring voltage V_i between electrodes when normal deformation is given to the pressure conductive rubber and amount of a voltage change ΔV when the rubber is shear deformed. However, the equation derived here changes depending on a dispersion or size for each lot of pressure conductive rubbers. When it is actually applied, it requires k and n to be experimentally determined for individual combinations.

5. Conclusions and Future Subjects

We attempted to make an experiment that an object was slipped in the configuration consisting of electrodes and a pressure conductive rubber to solve the cause of a peculiar output change appearing immediately before the object slipped on the CoP sensor. As a result, it was found that this peculiar output change was caused by a resistance change occurring when the pressure conductive rubber was shear deformed. It also became apparent that the amount of a resistance change by shear deformation was dependent largely on the shear deformation speed. Different from perpendicular deformation, shear deformation is not accompanied by a volume change. Therefore, it can be considered that this resistance change is caused by a particle distribution change in the pressure conductive rubber.

In the future, we will build up a slip sensor utilizing the characteristics of the pressure conductive rubber. To do so, we will make experiments to check to see how the output changes depending on a pressure conductive rubber type, differences in sensitivity, and an object to be slipped. To implement a slip sensor that uses the pressure conductive rubber to detect only a slip, it is necessary to separate an output change from that following an external force such as a normal force except a tangential force. We will consider an algorithm that separates a normal force from a slip.

References:

[1] R. S. Johansson and G. Westling, "Roles of glabrous skin receptors and sensorimotor memory in automatic control of precision grip when lifting rougher or more slippery objects," Exp. Brain Res., Vol.56, pp. 550-564, 1984.

[2] R. S. Johansson and G. Westling, "Signals in tactile afferents from the fingers eliciting adaptive motor responses during precision grip," Exp. Brain Res., Vol.66, pp. 141-154, 1987.

[3] M. R. Trembly and M. R. Cutkosky, "Estimating Friction using Incipient Slip Sensing During a Manipulation Task," Proc. IEEE Int. Conf. on Robotics and Automation, pp. 429-434, 1993.

[4] J. S. Son, E. A. Monteverde, and R. D. Howe, "A Tactile Sensor for Localizing Transient Events in Manipulation," Proc. IEEE Int. Conf. on Robotics and Automation, pp. 471-476, 1994.

[5] T. Maeno, K. Kobayashi, and N. Yamazaki, "Relationship between Structure of Finger Tissue and Location of Tactile Receptors," JSME Trans., Series C, Vol.63, No.607, pp. 881-888, 1997 (in Japanese).

[6] Y. Koda and T. Maeno, "Grasping Force Control in Master-Slave System with Partial Slip sensor," Proc. IEEE/RSJ Int. Conf. on Intelligent Robots and Systems, pp. 4641-4646, 2004.

[7] T. Maeno, S. Hiromitu, and T. Kawai, "Control of Grasping Force by Detecting Stick/slip Distribution at the Curved Surface of an Elastic Finger," Proc. IEEE Int. Conf. on Robotics and Automation, pp. 3895-3900, 2000.

[8] A. Ikeda, Y. Kurita, J. Ueda, Y. Matsumoto, and T. Ogasawara, "Grip force control for an elastic finger using vision-based incipient slip feedback," IEEE/RSJ Int. Conf. on Intelligent Robots and Systems, pp. 810-815, 2004.
[9] D. Gunji, Y. Mizoguchi, S. Teshigawara, A. Ming, A. Namiki, M. Ishikawa, and M. Shimojo, "Grasping Force Control of Multifingered Robot Hand Based on Slip Detection Using Tactile Sensor," Proc. IEEE Int. Conf. on Robotics and Automation, pp. 2605-2610, 2008.
[10] S. Teshigawara, M. Ishikawa, and M. Shimojo, "Slip Detection with Tactile sensor –Clarification of mechanism and Influence of coating material–," ROBOMEC2007, pp. 1A2-B09 (in Japanese).
[11] M. Shimojo, "Hysteresis Characteristics of Pressure-Conductive Rubber," JSME Trans., Vol.59, No.564, pp. 200-205, 1993 (in Japanese).
[12] M. Ishikawa and M. Shimojo, "A Method for Measuring the Center Position of a Two Dimensional Distributed Load Using Pressure-Conductive Rubber," SICE Trans., Vol.18, No.7, pp. 730-735, 1982 (in Japanese).
[13] Y. Tomita, "Rheology," CORONA PUBLISHING CO., pp. 92-94, 1975 (in Japanese).

Name:
Seiichi Teshigawara

Affiliation:
Master Course, Department of Mechanical Engineering and Intelligent Systems, The University of Electro-Communications

Address:
#515, 5F, Higashi#4 Building, 1-5-1 Chofugaoka, Chofu-shi, Tokyo 182-8585, Japan

Brief Biographical History:
2007- Master Course, Mechanical Engineering and Intelligent Systems, The University of Electro-Communications
2009- Doctoral Course, Mechanical Engineering and Intelligent Systems, The University of Electro-Communications

Main Works:
- S. Teshigawara, M. Ishikawa, and M. Shimojo, "Study of High Speed and High Sensitivity Slip Sensor –Characteristics of conductive material–," The SICE Annual Conference 2008, Japan, August 20-22, 2008.
- S. Teshigawara, M. Ishikawa, and M. Shimojo, "Development of High Speed and High Sensitivity Slip Sensor," IROS 2008, France, September 22-26, 2008.

Membership in Academic Societies:
- The Robotics Society of Japan (RSJ)
- The Japan Society of Mechanical Engineers (JSME)

Name:
Kenjiro Tadakuma

Affiliation:
Mechanical Engineering and Intelligent Systems, The University of Electro-Communications

Address:
#505, 5F, Higashi#4 Building, 1-5-1 Chofugaoka, Chofu-shi, Tokyo 182-8585, Japan

Brief Biographical History:
2002- Master Course, Tokyo Institute of Technology
2004- Doctoral Course, Tokyo Institute of Technology
2007- Postdoctoral Associate, Massachusetts Institute of Technology
2008- Postdoctoral Associate, Tohoku University
2008.4- Assistant Professor, The University of Electro-Communications

Main Works:
- K. Tadakuma, R. Tadakuma, and S. Hirose, "Mechanical Design of VmaxCarrier2: Omnidirectional Mobile Robot with Function of Step-Climbing," Journal of Robotics and Mechatronics, Vol.17, No.2, pp. 198-207, 2005.
- K. Tadakuma, M. Matsumoto, and S. Hirose, "Mechanical Design of Joint Braking and Underactuated Mechanism of "Tri-Star3"," The Int. Journal of Factory Automation, Robotics and Soft Computing, pp. 128-134, ISSN:1828-6984.
- K. Tadakuma, R. Tadakuma, and J. Berengueres, "Development of Holonomic Omnidirectional Vehicle with "Omni-Ball": Spherical Wheels," 2007 IEEE/RSJ Int. Conf. on Intelligent Robots and Systems (IROS 2007), IEEE Catalog Number: 07CH37863D, ISBN:1-4244-0912-8.

Membership in Academic Societies:
- The Institute of Electrical and Electronics Engineers (IEEE)
- The Robotics Society of Japan (RSJ)

Name:
Aiguo Ming

Affiliation:
Associate Professor, Department of Mechanical Engineering and Intelligent Systems, University of Electro-Communications

Address:
1-5-1 Chofugaoka, Chofu-shi, Tokyo 182-8585, Japan

Brief Biographical History:
1990 Received the Ph.D. from The University of Tokyo
1990 Joined Mitutoyo Corporation
1991 Joined Yamanashi University
1994 Joined The University of Electro-Communications

Main Works:
- "Design for high performance robot based on dynamically-coupled driving and joint stops," Int. J. Robotics & Automation, Vol.22, No.4, pp. 281-293, December 2007.
- "Adaptive Robust Motion/Force Control of Holonomic-Constrained Nonholonomic Mobile Manipulators," IEEE Transactions on Systems, Man, and Cybernetics, Part B, Vol.37, No.3, pp. 607-616, June 2007.

Membership in Academic Societies:
- The Institute of Electrical and Electronics Engineers (IEEE)
- The Robotics Society of Japan (RSJ)
- The Society of Instrument and Control Engineers (SICE)
- The Japan Society of Mechanical Engineers (JSME)
- The Japan Society for Precision Engineering (JSPE)

Name:
Masatoshi Ishikawa

Affiliation:
Professor, Department of Mathematical engineering and Information physics, Faculty of Engineering, The University of Tokyo

Address:
#251, 2F, Department of Engineering #6 Building, 7-3-1 Hongo, Bunkyo-ku, Tokyo 113-0033, Japan

Brief Biographical History:
1979-1989 Senior Researcher at Industrial Products Research Institute, Tsukuba, Japan
1989-1999 Associate Professor with the Department of Mathematical Engineering and Information Physics, University of Tokyo
2001- Professor of information physics and creative informatics at the University of Tokyo

Name:
Makoto Shimojo

Affiliation:
Professor, Department of Mechanical Engineering and Intelligent Systems, The University of Electro-Communications

Address:
1-5-1 Chofugaoka, Chofu, Tokyo 182-8585, Japan

Brief Biographical History:
1976-1992 Senior Researcher at Industrial Products Research Institute, Tsukuba, Japan
1993-1997 Senior Researcher at National Institute of Bioscience and Human Technology, Tsukuba, Japan
1985-1986 Visiting Scholar at Stanford University, U.S.A.
1997-2001 Professor of Computer and Information Sciences at Ibaraki University
2001- Professor, Department of Mechanical Engineering and Intelligent Systems, The University of Electro-Communications

Main Works:
- M. Shimojo, M. Shinohara, and Y. Fukui, "Human Shape Recognition Performance for 3D Tactile Display," IEEE Transaction on Systems, Man and Cybernetics, Part A, Vol.29, No.6, pp. 637-644, 1999.
- M. Shimojo, A. Namiki, M. Ishikawa, R. Makino, and K. Mabuchi, "A tactile sensor sheet using pressure conductive rubber with electrical-wires stitched method," IEEE Trans. Sensors, Vol.5, No.4, pp. 589-596, 2004.

Membership in Academic Societies:
- The Robotics Society of Japan (RSJ)
- The Society of Instrument and Control Engineers (SICE)
- The Japan Society of Mechanical Engineers (JSME)
- Virtual Reality Society of Japan (VRSJ)
- The Institute of Electronics, Information and Communication Engineers (IEICE)

A High-Speed Mesh of Tactile Sensors Fitting Arbitrary Surfaces

Makoto Shimojo, Takuma Araki, Aigou Ming, *Member, IEEE*, and Masatoshi Ishikawa

***Abstract*—A tactile sensor is developed with the aim of covering a robot's entire structure, while reducing wiring requirement and ensuring high-speed response. The sensor detects the center point of load distribution on 2-D surfaces as well as the overall load. There are only four signal wires from the sensor. The sensor response time is nearly constant (within 1 ms) regardless of the number of detection elements, their placements or sensor areas. In this paper, the principles behind the operation of this sensor and the results of experiments using the sensor are described.**

***Index Terms*—High-speed response, mesh structure, reducing wiring, robot skin, tactile sensing.**

I. Introduction

AMONG many researches done on tactile sensors, many of them are about sensors for attaching to the hands of robots for the purpose of gripping and manipulating their hands [1], [2]. Recently, however, with the increased interest on research and development of robots in human-like form, research on the development of tactile sensors covering the whole body of the robot itself has become popular [3]–[5]. Although the applications for which these researches are intended do not require high spatial resolution of these sensors, they do require that the sensors be attachable to arbitrary surfaces that can cover a wide area. Moreover, rapid response is desired to ensure safety. Because these full body skin tactile sensors cover a wide area, the detection elements need to be spread over a wide range which in turn requires a lot of wiring for signal transmission. For this reason, when sensors are attached to movable parts such as the wrists and fingers, many problems occur from design limitations due to restrictions on movement imposed by the wirings [6]. Several studies have been done to solve these problems. We would like to introduce some of these attempts as follows.

First, tactile sensors have been developed by Inaba *et al.* where the number of wirings is the same as the number of detection elements [7]. This structure uses a mesh-structure spacer sandwiched between conductive sheets. When load is applied, the conductive sheets come into contact through the mesh to detect load. This developed sensor is flexible and can cover a wide area. However, the number of wirings increases as the area covered becomes larger.

Next, some tactile sensors have been developed with the matrix arrayed system. In this structure, the detection elements are placed on the intersection of the vertical and horizontal lines. The detection element is identified from the intersection of the row and column. This structure requires $(m+n)$ lines of wiring for an $(m \times n)$ matrix. For example, Seki *et al.* developed a glove-structured sensor for the purpose of measuring the grip of humans [8]. In this structure, conducting wires are sewn alternately along horizontal and vertical directions on pressure conductive rubber. While this sensor is flexible and durable, many wiring restricts free finger motion. Another type developed is a sensor made of sheets printed with stripes of pressure sensitive ink. Two sheets are laid over each with the stripes on one sheet along the horizontal and the other the vertical direction [9]. The intersections of the horizontal and vertical stripes serve as the pressure sensitive area. A stripe is as thin as about 0.1 mm, it is possible to realize high spatial resolution. However, the sensor is sheet like form, it is hard for the sensor to cover a curved surface.

Recently, a method called Electrical Impedance Tomography (EIT) was developed. Electrodes are arranged at the periphery of a conductive sheet. And the distribution of the resistance inside the conductive sheet is measured using inverse problem method [10]. Since there is no need for wiring inside the measurement area, the sensor can be made flexible, thin and extensible. However, on the other hand, a large number of electrodes may be needed to increase spatial resolution.

Other sensors developed uses serial bus as a way to reduce wiring. For example, Ohmura *et al.* proposed the reduction in the number of wirings by arranging a MPU (micro processing unit) on a sensor sheet with 32 pressure sensitive parts considered as a unit and combining high-speed serial buses of each sensor sheet [11]. However, scanning time problems results from the increase in number of elements. Other sensor types proposed are such as that: multiplexes the signal from the detection elements via spread spectrum transmission method [12], sequentially transmits the signal from detection elements through one line using delay circuitry [13]. Shinoda *et al.* proposed a very unique wireless technique through the use of a sensor chip whose transmission frequency changes with load. This sensor chips were dispersed under a flexible form that was formed to the desired shape, and transmission of power and signal is done through an external coil [14]. However, their development is now at a stage of the first trial prototype.

Manuscript received April 15, 2009; revised October 08, 2009; accepted October 08, 2009. Current version published March 10, 2010. The associate editor coordinating the review of this paper and approving it for publication was Prof. Evgeny Katz.

M. Shimojo, T. Araki, and A. Ming are with the Department of Mechanical Engineering and Intelligent Systems, University of Electro-Communications, Tokyo,182-8585 Japan (e-mail: shimojo@mce.uec.ac.jp; ming@mce.uec.ac.jp).

M. Ishikawa is with the Department of Information Physics and Computing, Graduate School of Information Science and Technology, University of Tokyo, Tokyo 113-8656, Japan (e-mail: ishikawa@k2.t.u-tokyo.ac.jp).

Digital Object Identifier 10.1109/JSEN.2009.2034982

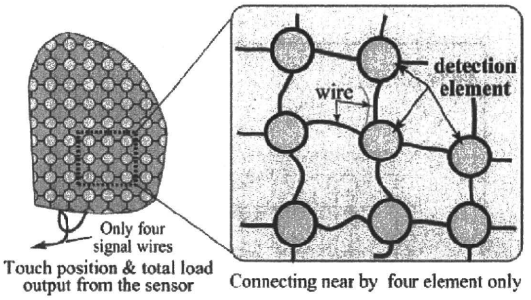

Fig. 1. Outline of the sensor. Net-like structure and only four output lines from the sensor.

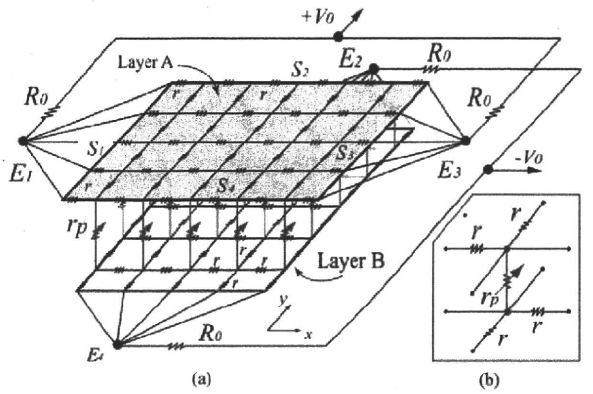

Fig. 2. Structure of the sensor. A detector layer is sandwiched by $m \times n$ matrix arrayed resistor layers. (a) Three layered structure. (b) Detection element.

There are many other researches going on other than those mentioned above [15]. But these have a common problem described as follows.

1) Mounting on arbitrary surfaces: Many of the tactile sensors currently developed are of the sheet variety and cannot be mounted on arbitrary surfaces.
2) Excessive wiring: A lot of wiring are required for many detection elements when covering a wide area.
3) Sluggish response due to scanning: Since the number of detection elements becomes too many, scanning of every detection element results to delayed response time.

In this study, a mesh of tactile sensors that can be attached to arbitrary surfaces with reduced wiring requirement and rapid response was developed. The conceptual outline of the sensor is shown in Fig. 1. The sensor is formed into a structure resembling a net. It can be attached to arbitrary surfaces, and can detect the center of the load distribution as well as the overall load on 2-D surfaces. There are only four output lines from the sensor and internal connection is required only between adjacent detection elements. Moreover, since the sensor structure is analog circuit, the response speed is almost constant regardless of the number of detection elements, placement and surface area of the sensor. In summary, the sensor features the following.

1) Covers arbitrary surfaces: the sensor can be laid out like a net to cover arbitrary surfaces.
2) Reduced wiring: Lines from the sensor consist of four wires only regardless of number, surface area, or placement of detection elements.
3) High-speed response: Response time is less than 1 ms without regard to the number of detection elements which means that the sensor is adequate for use in control loops around 1 kHz; the standard used in robotics control.

II. Sensor Structure

The structure of the sensor is shown in Fig. 2. As shown in this figure, the structure is a three-layered structure. Layer A is a $m \times n$ arrayed resistors. All resistors at the left end of layer A are connected to electrode E_1 which is connected to a voltage of $+V_0$ through the external resistor R_0. In like manner, all resistors at the right end are connected to the electrode E_3 and are connected to a voltage of $+V_0$. The network structure of layer B is the same as that of layer A. However, the electrode connections of layer B are found at the upper and lower ends unlike in the case of layer A. Layers A and B are connected by detection element r_p whose resistance varies with the load. Fig. 2(b) shows a unit element. The output of the sensor consists of the voltages from the four electrodes, E_1, E_2, E_3, E_4. The advantages gained from this kind of a structure are: 1) Sensor size can be varied easily by connecting any number of elements sequentially along the horizontal and vertical directions on the $m \times n$ matrix. 2) The unit detection element r_p can be replaced if the electrical resistance or electrical current changes with the physical value. For example, if a photo-reflector is used instead of pressure-conductive rubber, distance is detectable instead of force. That is, the sensor can be used easily not only as a 2-D load sensor but also as a 2-D proximity sensor. 3) Since the adjacent unit elements are connected into a net-structure, it is possible to cover arbitrary surfaces in the same way as covering an object with a net.

III. Sensor Principle

The detection element r_p changes its electrical resistance with load. When load is applied to the sensor, the value of the resistance r_p drops and the value of the electrical current increases. That is, in other words, the distribution of the load on the sensor is converted into the distribution of the electrical current flowing from layer A to layer B. For this sensor, the center of the load distribution can be detected as the center of the current distribution [16], [17].

A. Equivalent Circuit and Basic Equation

Fig. 3 shows the equivalent circuit at the neighborhood of a unit element. Current flowing from layer A to layer B through the resistor $r_p(i,j)$ is set to $I(i,j)$. The voltage $V_a(i,j)$ and $V_b(i,j)$ are the voltage of the corresponding nodes on layers A and B respectively. Applying Kirchhoff's current law on the layer A, the current flowing through the node indicated by the voltage $V_a(i,j)$ is equal to the current $I(i,j)$ passing through the resistor $r_p(i,j)$ as shown in Fig. 3. Thus, the following equation can be established:

$$\frac{1}{r}\{V_a(i-1,j)+V_a(i+1,j)+V_a(i,j-1) +V_a(i,j+1)-4V_a(i,j)\}=I(i,j). \quad (1)$$

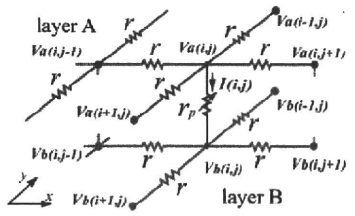

Fig. 3. Equivalent circuit at the neighborhood of a detection element.

Replacing the left side of (1) with the discrete Laplace operator ∇^2, (1) can be written as (2) [18]

$$\frac{1}{r}\nabla^2 V_a(i,j) = I(i,j). \tag{2}$$

Using the same method, the following equations can be derived for layer B:

$$\frac{1}{r}\nabla^2 V_b(i,j) = -I(i,j). \tag{3}$$

B. Position Coordinates of the Detector Element

Fig. 4 shows the position coordinate for the placement of a detector element. The detector elements are assumed to be distributed equally. Further, it is assumed that origin of $x_{i,j}$ falls on the center of the sensor. In order to satisfy these assumptions, $x_{i,j}$ is defined in (4), thus

$$x_{i,j} = \frac{2j-(n+1)}{n-1} \quad (-1 \le x_{i,j} \le +1). \tag{4}$$

Also, for y direction position coordinate $y_{i,j}$, set as defined in (5)

$$y_{i,j} = \frac{-2i+m+1}{m-1} \quad (-1 \le y_{i,j} \le +1). \tag{5}$$

In this manner of setting the coordinates, the placement of the detector elements form a matrix with uniform intervals and the position coordinates $x_{i,j}, y_{i,j}$ for all detector elements form an arithmetic progression. The Laplace operator then becomes zero as shown in (6)

$$\nabla^2 x_{i,j} = \nabla^2 y_{i,j} = 0. \tag{6}$$

This relationship will be used in Section III-D.

C. Boundary Conditions

Considering the electrical boundary conditions for the sensor shown in Fig. 4, the boundaries S_2 and S_4 of layer A do not have any external contact so that these layers are open terminals. Hence, no current flows from the outside and the voltage does not change. The boundary conditions therefore are shown, as in (7)

$$V_a(0,j) = V_a(1,j), \quad V_a(m+1,j) = V_a(m,j). \tag{7}$$

Next, let us consider the boundaries S_1 and S_3 for layer A which are connected to the electrodes E_1 and E_3, respectively, such

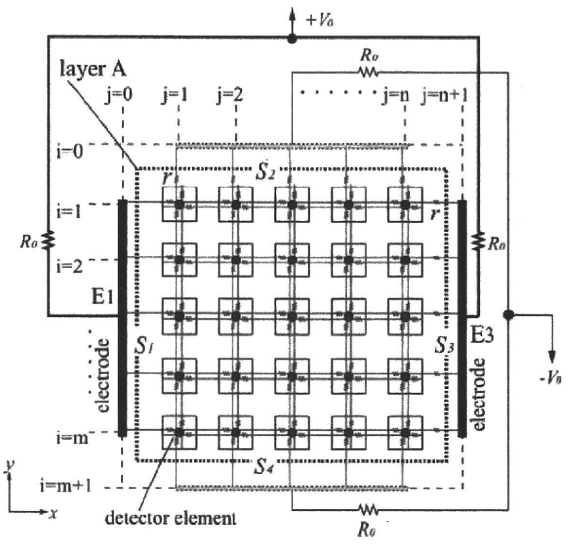

Fig. 4. Position of a detector element in layer A and electrical boundary conditions for the sensor.

that current flows in from the electrodes. This current passes through the externally connected resistor R_0. Hence, the value of this current can be determined from the voltage drop between the ends of R_0. Since the total of the currents that passes through the detector elements are equal to current that flows through R_0, (8) and (9) are established as follows:

$$\frac{1}{R_0}\{V_0 - V_{E1}\} = \frac{1}{r}\left\{\sum_{i=1}^{m}(V_{E1} - V_a(i,1))\right\} \tag{8}$$

$$\frac{1}{R_0}\{V_0 - V_{E3}\} = \frac{1}{r}\left\{\sum_{i=1}^{m}(V_{E3} - V_a(i,n))\right\}. \tag{9}$$

Further, since $j = 0$ for electrode E_1 and $j = n+1$ for electrode E_3, the boundary conditions becomes as

$$V_a(i,0) = V_{E_1}, \quad V_a(i,n+1) = V_{E_3}. \tag{10}$$

Since layer B is similarly situated, the boundary conditions for this layer are similarly established, as in (7)–(10).

D. Total Current and Center of the Current Distribution

To determine the center of the distribution of the current value, it is necessary to determine the primary moment of current distribution with respect to the x direction. This primary moment I_x with respect to the x direction of the $m \times n$ matrix formed by the detector elements can be expressed as (11)

$$I_x = \sum_{i=1}^{m}\sum_{j=1}^{n} x_{i,j} I(i,j). \tag{11}$$

Replacing current $I(i,j)$ with (2) in the equation above gives (12) as follows:

$$I_x = \frac{1}{r}\sum_{i=1}^{m}\sum_{j=1}^{n} x_{i,j}\nabla^2 V_a(i,j). \tag{12}$$

Expanding the Laplace operator ∇^2 of (12) results to (13), which in turn can be expressed as in (14) with expanding and organizing it

$$I_x = \frac{1}{r}\left\{\sum_{i=1}^{m}\sum_{j=1}^{n} x_{i,j}V_a(i-1,j) + \sum_{i=1}^{m}\sum_{j=1}^{n} x_{i,j}V_a(i+1,j) + \sum_{i=1}^{m}\sum_{j=1}^{n} x_{i,j}V_a(i,j-1) + \sum_{i=1}^{m}\sum_{j=1}^{n} x_{i,j}V_a(i,j+1) - 4\sum_{i=1}^{m}\sum_{j=1}^{n} x_{i,j}V_a(i,j)\right\} \quad (13)$$

$$I_x = \frac{1}{r}\left\{\sum_{i=1}^{m}\sum_{j=1}^{n} V_a(i,j)\nabla^2 x_{i,j} + \sum_{j=1}^{n}(x_{m,j}V_a(m+1,j) - x_{m+1,j}V_a(m,j)) + \sum_{j=1}^{n}(x_{1,j}V_a(0,j) - x_{0,j}V_a(1,j)) + \sum_{i=1}^{m}(x_{i,n}V_a(i,n+1) - x_{i,n+1}V_a(i,n)) + \sum_{i=1}^{m}(x_{i,1}V_a(i,0) - x_{i,0}V_a(i,1))\right\}. \quad (14)$$

Next, let us apply the proper position coordinates and the boundary conditions to (14) and simplify the result. Firstly, the first item in (14) can be reduced to zero by applying the position coordinates settings defined by (6). Next, since $x_{i,j}$ is the function only for j, therefore, it is constant toward the direction of i, that is, $x_{m,j} = x_{m+1,j}$. With the boundary conditions given by (7), the second and third items of (14) become zero and (14) simplifies into the following equation:

$$I_x = \frac{1}{r}\left\{\sum_{i=1}^{n}(x_{i,n}V_a(i,n+1) - x_{i,n+1}V_a(i,n)) + \sum_{i=1}^{n}(x_{i,1}V_a(i,0) - x_{i,0}V_a(i,1))\right\}. \quad (15)$$

Applying the boundary conditions given by (8) and (9) to (15) and imposing the boundary conditions given by (10) further results to (16) below

$$I_x = \frac{1}{n-1}\left(\frac{2m}{r} + \frac{n+1}{R_0}\right)\cdot(V_{E_1} - V_{E_3}). \quad (16)$$

In like manner, the primary moment I_y with respect to the y direction can be expressed in the following equation:

$$I_y = \frac{1}{m-1}\left(\frac{2n}{r} + \frac{m+1}{R_0}\right)\cdot(V_{E_2} - V_{E_4}). \quad (17)$$

Here, m, n, r and R_0 are constants. Hence, I_x can be computed as a constant multiplier of the voltage potential difference (E_1, E_3) between the electrodes of layer A. Similarly, I_y can be determined from the voltage potential difference (E_2, E_4) between the electrodes of layer B. Moreover, since the total current flowing from layer A to layer B is the current that flows through R_0, the total current I_{all} is given by (18)

$$I_{\text{all}} = \sum_{i=1}^{m}\sum_{j=1}^{n} I(i,j) = \frac{2V_0 - V_{E_1} - V_{E_3}}{R_0} = \frac{2V_0 + V_{E_2} + V_{E_4}}{R_0}. \quad (18)$$

With the above, the center of the current distribution defined as x_0 and y_0, can now be determined from (19)

$$x_0 = (I_x)/(I_{\text{all}}), y_0 = (I_y)/(I_{\text{all}}). \quad (19)$$

E. Numerical Modeling of the Load Distribution

The previous discussion established that the total current and the center of the current distribution can be determined from the voltage difference between the electrodes. In this section, we shall investigate the relationship between current $I(x,y)$ and the resistance of the pressure sensitive element $r_p(i,j)$. Let us consider layer A first. The current $I(x,y)$ flowing through $r_p(i,j)$ as shown in Fig. 3 can be expressed as (20)

$$I(i,j) = \frac{1}{r_p(i,j)}(V_a(i,j) - V_b(i,j)). \quad (20)$$

With this, (1) becomes

$$\left\{4 + \frac{r}{r_p(i,j)}\right\}[V_a]_{i,j} - [V_a]_{i-1,j} - [V_a]_{i+1,j} - [V_a]_{i,j-1} - [V_a]_{i,j+1} - \frac{r}{r_p(i,j)}[V_b]_{i,j} = 0. \quad (21)$$

Next, let us consider the boundary conditions. From (8), and considering electrode E_1

$$\left(1 + \frac{R_0}{r}m\right)V_{E1} = V_0 + \frac{R_0}{r}\sum_{i=1}^{m} V_a(i,1). \quad (22)$$

Similarly, from (9) and considering electrode E_3

$$\left(1 + \frac{R_0}{r}m\right)V_{E3} = V_0 + \frac{R_0}{r}\sum_{i=1}^{m} V_a(i,n). \quad (23)$$

Equations similar to those for layer A can likewise be established for layer B. The equations for each point in layers A and B and the equations for each electrode E_1, E_2, E_3, and E_4 above, when taken altogether, form $(2mn+4)$ simultaneous equations. These equations serve as the numerical model for the sensor.

F. Total Load and Center of Load Distribution

In this section, the relationship between current $I(i,j)$ and load $F(i,j)$ is investigated. Let us suppose that, for this sensor,

resistance r_p and load $F(i,j)$ are inversely related, as shown in (24)

$$r_p(i,j) = kF^{-1}(i,j) \tag{24}$$

where, k is a constant. Here, if the resistance r is much lower than resistance r_p ($r_p \gg r$), the voltage drop due to r would be very small. This means that we can say that the voltages at layers A and B, $V_a(i,j)$ and $V_b(i,j)$, are practically constant. Eq. (20) thus becomes (25)

$$I(i,j) = \frac{V_a(i,j) - V_b(i,j)}{r_p(i,j)} \approx \frac{V_A - V_B}{r_p(i,j)}. \tag{25}$$

From this, we can say that the current $I(i,j)$ and the load $F(i,j)$ are directly proportional as (26) indicates

$$I(i,j) = \frac{(V_A - V_B)}{k} F(i,j). \tag{26}$$

Consequently, the center of load distribution is the same as the center of the current distribution, x_0 and y_0 defined by (27) and (28)

$$x_0 = \frac{\sum_{i=1}^{m}\sum_{j=1}^{n} x_{i,j}F(i,j)}{\sum_{i=1}^{m}\sum_{j=1}^{n} F(i,j)} = \frac{I_x}{I_{\text{all}}} \tag{27}$$

$$y_0 = \frac{\sum_{i=1}^{m}\sum_{j=1}^{n} y_{i,j}F(i,j)}{\sum_{i=1}^{m}\sum_{j=1}^{n} F(i,j)} = \frac{I_y}{I_{\text{all}}}. \tag{28}$$

Moreover, since V_A and V_B are assumed to be practically constant, V_A is the average of V_{E1} and V_{E3}, while V_B is the average of V_{E2} and V_{E4}. Using these values, total load will be (29)

$$F_{\text{all}} = \sum_{i=1}^{m}\sum_{j=1}^{n} F(i,j) \approx \frac{2kI_{\text{all}}}{(V_{E1} + V_{E3} - V_{E2} - V_{E4})}. \tag{29}$$

IV. Simulation

The sensor consists of r, R_0 and r_p. Among them, r_p is decided from an actual detector. However, r and R_0 are parameters determined by the designer. Therefore, how r and R_0 affects the sensor characteristics is established from simulation.

A. Simulation Model

The numerical model of the sensor is made up of $(2mn + 4)$ simultaneous algebraic equations established in Section III-E and shown in (30)

$$\boldsymbol{S}\boldsymbol{v} = \boldsymbol{c}. \tag{30}$$

Here, $\boldsymbol{v}$ represents the voltage, $V_a(i,j)$ and $V_b(i,j)$, respectively, and $\boldsymbol{c}$ represents the external applied voltage $\pm V_0$. Both are $(2nm + 4)$ dimensional vectors. Moreover, $\boldsymbol{S}$ represents a $(2nm + 4) \times (2nm + 4)$ coefficient matrix. The value of $\boldsymbol{S}$ is determined from (21) with the boundary conditions defined by (22) and (23). The numerical solution to the equations of (30) was obtained using MATLAB.

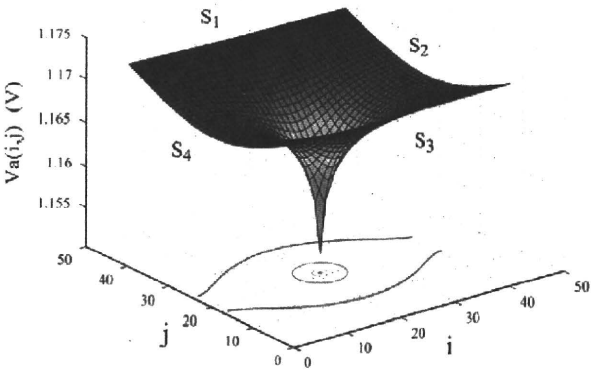

Fig. 5. Voltage $V_a(i,j)$ on the layer A with one point load. Elements are arranged in 41×41 grid, $V_0 = 15$ V, $R_0 = 10\text{k}\,\Omega$, $r = 10\,\Omega$, $r_p = 864\,\Omega$ ($F_0 = 5$ N).

B. Effect of Network Resistance R

In this section, we will establish the relationship between the resistance r and sensor properties. First, let us look at an example of the simulation results for the voltage distribution in layer A shown in Fig. 5. In this case, a single load of $F_0 = 5$ N is applied at the center of the sensor. In the simulation, the voltage drop due to r is less than 0.02 V. It is very small.

In Section III-F, We suppose that resistance $r_p(i,j)$ and load $F(i,j)$ are inversely related and the resistance r is much lower than resistance r_p as shown in (31). Then, the center of load distribution is the same as the center of the current distribution, x_0 and y_0 defined by (27) and (28)

$$1 \gg r/r_p. \tag{31}$$

This assumption was verified by the simulation. Simulation was conducted with the values of r set at 10 Ω, 47 Ω, 100 Ω, and 150 Ω. The result is shown in Fig. 7. The figure clearly shows that when r increases, the voltage distribution of $V_a(i,j)$ changes. In Fig. 7, when r is 10 Ω, voltage $V_a(i,j)$ can be considered practically constant. However, as the value of r increases, the value of $V_a(i,j)$ tends to vary from a constant value. Also, although the polarity of voltage $V_b(i,j)$ is opposite to $V_a(i,j)$, the same changes occur in $V_b(i,j)$. As a result, the condition that $(V_a(i,j) - V_b(i,j))$ should be constant is no longer satisfied. It means that the current $I(i,j)$ and the load $F(i,j)$ are not proportional as (26) indicates. Therefore, it cannot be considered that the center of current distribution is the same as the center of load distribution.

Especially, this effect becomes a problem when multiple loads are applied on the sensor. As an example, Fig. 6 shows what happens when loads are applied on three points. It was assumed that the total of the loads on the three points is 5 N. As clearly shown in the figure, loading positions affected voltage distribution $V_a(i,j)$ so that $(V_a(i,j) - V_b(i,j))$ changed. This indicates that the location where load is applied affects the sensor output. The following section will investigate these effect.

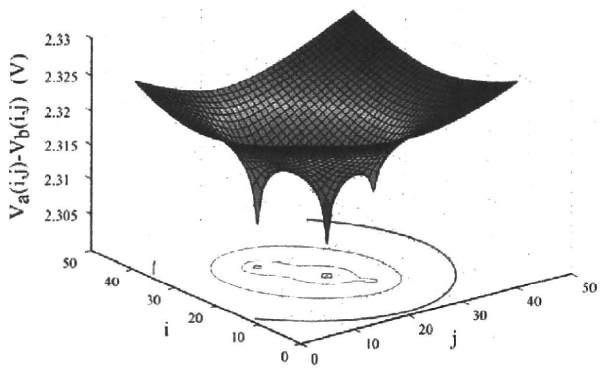

Fig. 6. Voltage of the $(V_a(i,j) - V_b(i,j))$ by the three-point load. Elements are arranged in 41 × 41 grid, $V_0 = 15$ V, $R_0 = 10k\ \Omega$, $r = 10\ \Omega$, Total load = 5 N.

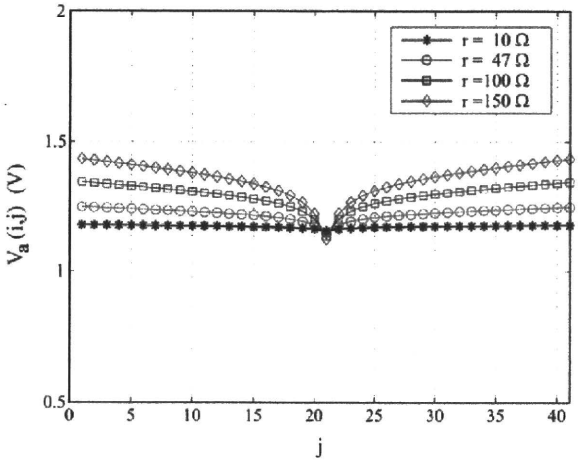

Fig. 7. Change of the $V_a(i,j)$ with resistance "r". Elements are arranged in 41 × 41 grid, $V_0 = 15$ V, $R_0 = 10$ k Ω, $r_p = 864\ \Omega$ ($F_0 = 5$ N).

TABLE I
CHANGE OF r/r_p BY INPUT LOAD. ($k = 4320$ [N Ω])

load \ r	10 Ω	47 Ω	100 Ω	150 Ω
5 N	0.0115	0.0544	0.1157	0.1736
10 N	0.02315	0.01088	0.2315	0.3472
15 N	0.03472	0.1632	0.3472	0.5208
20 N	0.04630	0.2178	0.4629	0.6944

C. Verification of Sensor Output Error

The measurement error increases according to the increase in r. This is because the ratio r/r_p increased. However, when F increases, (24) states that r_p decrease. As a result, the ratio r/r_p increases. Table I shows the result of computing the ratio r/r_p when r_p is changed by input force F.

Hence, simulation was done to determine the measurement error when the load $F(i,j)$ and r are made to change. Simulation of the sensor output when the loads are applied on multiple points was conducted. Six loading points were considered in the simulation. The conditions in the simulation were, random load position with six loading positions and total loads of 5 N, 10 N, 15 N and 20 N. Moreover, the computations were done for values of r of 10 Ω, 47 Ω, 100 Ω, and 150 Ω. One-hundred computation runs per simulation condition were performed. The sensor error was shown by the average and standard deviations. Fig. 8 shows the position output error while Fig. 9 shows the total load error. The vertical axis of Fig. 8 represents the ratio of the position output error while that for Fig. 9 represents the ratio of the sensor output error for total load. Further, the horizontal axis for both figures represents the total load. It is clear that an error increases as total load increases. However, the results of the simulation described above show that for $r = 10\ \Omega$, the position error is within 0.5% while that for total load was within 2%. It means that this sensor operates with sufficient accuracy when r/r_p is less than 0.05.

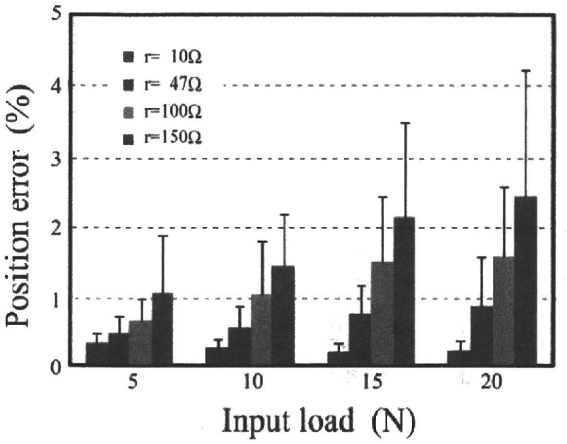

Fig. 8. The position output error by change of the total load. Elements are arranged in 41 × 41 grid, $V_0 = 15$ V, $R_0 = 10$ k Ω, loading point: random, number of loading = 6.

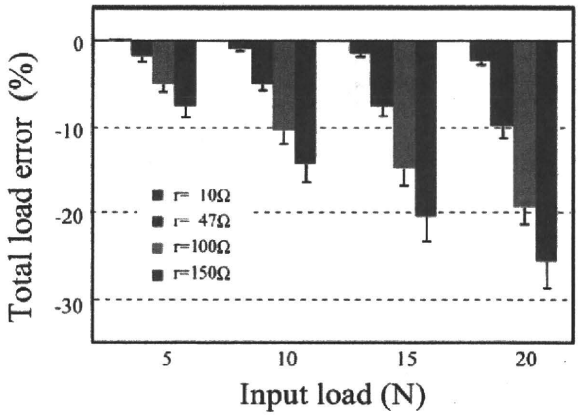

Fig. 9. The total load output error by change of the total load. Elements are arranged in 41 × 41 grid, $V_0 = 15$ V, $R_0 = 10$ k Ω, loading point: random, number of loading = 6.

D. Effect of Resistance $r0$

It is clear from sensor structure shown in Fig. 2 that as R_0 increases, the total current I_{all} decreases. At the same time, the voltage drop due to R_0 increases, thus the voltage of $(V_a(i,j) - V_b(i,j))$ becomes smaller. At the same, the voltage differences between electrodes, $(V_{E_1} - V_{E_3})$ and $(V_{E_2} - V_{E_4})$ become

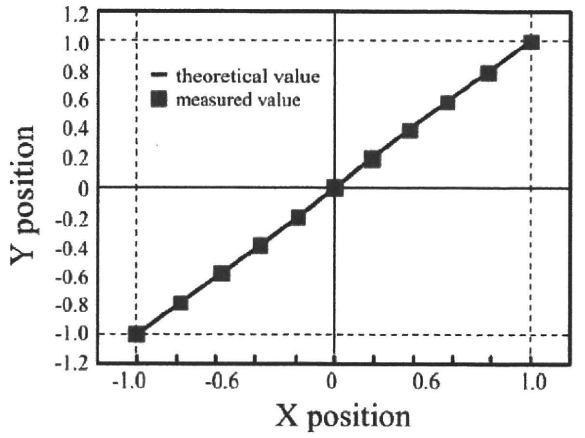

Fig. 10. Experimental result of the position output by two-point load.

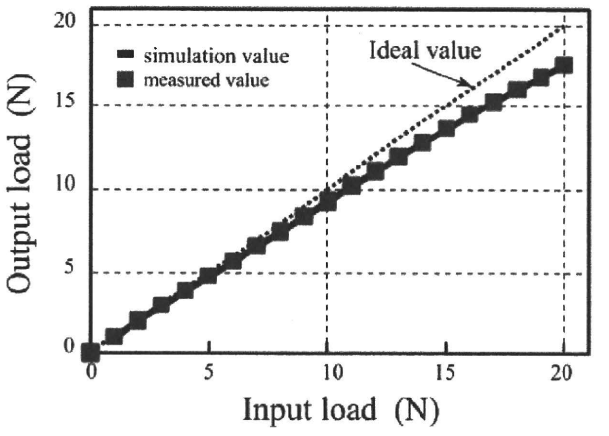

Fig. 11. Experimental result of the total load output by two-point load.

small. These results mean that the S/N ratio of the sensor will decrease in the electrical noise environments. However, it was shown in this simulation that error of the position and the total load output were not affected by a change in the external resistance R_0.

V. Prototype Validation of Sensor Properties

In this section, the behavior of a prototype sensor was verified. The sensor is an electrical circuit made up of resistances only. The sensor is constructed of network resistance r and detector element r_p. For example, as a material that the resistance changes with force, a pressure conductive rubber may be used. However, pressure conductive rubber undergoes hysteresis and creep etc. Thus, uncertainties in the relationship between the load and resistance exist. Hence, a quantitative evaluation of this sensor is difficult. For this reason, adjustable resistors were used as detector element r_p. In the experiment, elements were arranged in 5×5 grid. The circuit constants were assigned as: $r = 47\ \Omega$ and $R_0 = 10$ k Ω. Moreover, the load and resistance r_p were assumed to satisfy the relationship defined by (24), and k was set to 4320 [N Ω].

A. Position Measuring Experiment

The sensor is able to detect the center of the load distribution. A validation experiment was conducted on the position output under two point loading. The sensor outputs the center position of the load distribution. First of all, loads F_1 and F_2 were applied at the sensor coordinate positions $(-1.0, -1.0)$ and $(+1.0, +1.0)$. Then the sensor position output was measured. In the experiment, the sum $F_1 + F_2 = 10$ N was fixed. F_1 was made to change from 0 N to 10 N with 1 N-increments. Hence, the sensor position output must be changed by steps from $(-1.0, -1.0)$ to $(+1.0, +1.0)$. The results of the experiment are shown in Fig. 10. With an increase in load, the sensor output correctly moved the straight lines connecting the load positions. The figure shows that the simulation results and the measured values agree very well.

B. Load Measurement Experiment

The sensor also can be used to output the total value of the distributed loads. Two loads, F_1 and F_2, were applied on the coordinate positions $(0, 0)$ and $(+0.5, +0.5)$ and the sensor load outputs were measured. During the experiment, $(F = F_1 = F_2)$ and F was made to vary from 0 N to 10 N with 0.5 N-increments. The results of the experiment are shown in Fig. 11. The figure shows that the simulation results and the measured values agree very well. However, Fig. 11 also clearly shows that as the load increases, the measured values departed from the ideal values. This difference is the influence of the two load which affected each other, as shown in Fig. 6.

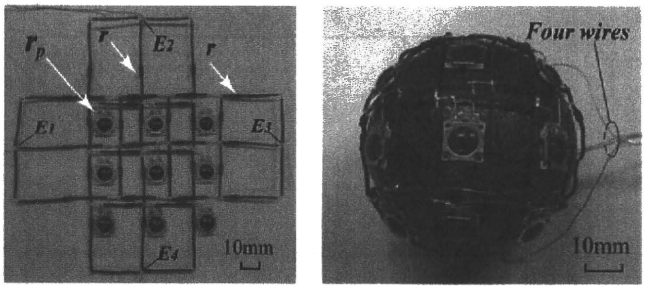

(a) (b)

Fig. 12. Prototype of the mesh of tactile sensors. Detector elements are pressure conductive rubber arranged in 3×3 grid. (a) View of the sensor. (b) Attached on semi-sphere.

VI. Sensor Prototype Using Pressure Conductive Rubber

Fig. 12 shows the prototype of a sensor. The prototype sensor used a pressure-conductive rubber manufactured by Inaba Rubber Company, Ltd., as the detector element r_p. The elements were arranged in a 3×3 grid. The resistance r was set to $r = 47\ \Omega$. As the sensor has a net-structure, it can be mounted on a sphere as shown in Fig. 12(b).

A. Response to Impulse Load

The sensor was tested to measure the time of the response. The experiment was conducted to apply an input load on the sensor by an Impulse Hammer (Ono sokki, GK-300) and to measure the time until the sensor outputs a constant voltage corresponding to the input position. Fig. 13 shows the time response of the position output just after the input load is applied. As

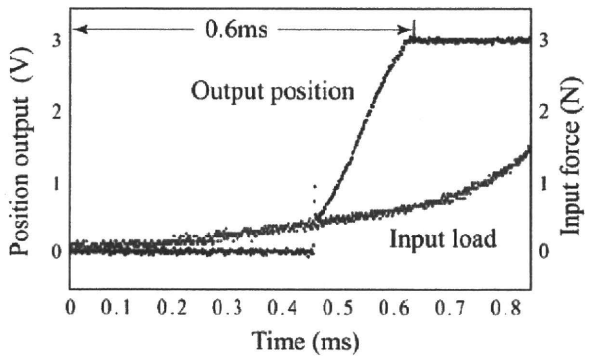

Fig. 13. Time response of the position output just after the input load is applied.

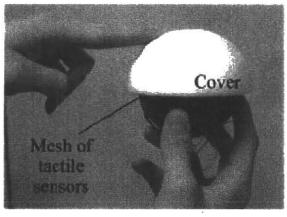

Fig. 14. Photograph of the stroking experiment with sensor covered by styrene foam.

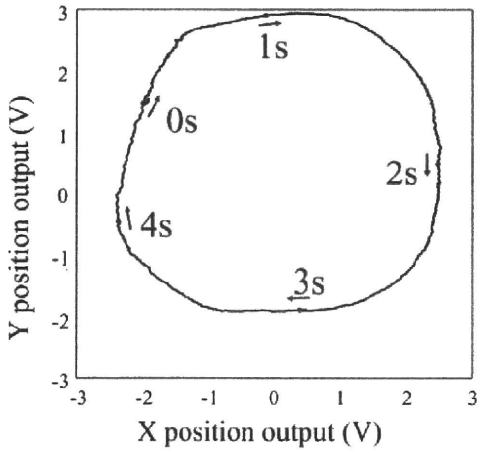

Fig. 15. A locus of the sensor's position output. The cover top is pushed by a fingertip drawing a circle.

shown in the figure, it took about 0.6 ms to output the input position after the load is applied. In general, the sensor feedback control cycle is 1 ms or less. The sensor is adequate for use in control loops around 1 kHz; the standard used in robotics control.

B. Semi-Spherical Surface Attachment Experiment

Fig. 14 shows detector elements arranged on a semi-spherical surface and these elements were covered by a semi-spherical styrofoam [19]. Fig. 15 shows the sensor output when the cover top is pushed so that a circle may be drawn by a fingertip. It can be seen from the figure that a neat locus is formed. Even when the elements are arranged discretely, the output can be obtained continuously through the use of a cover serving as sensor's skin.

VII. Summary

A mesh of tactile sensors is developed with the aim of covering a robot's entire structure, while reducing wiring requirement and ensuring high-speed response. The sensor has a net-structure, can cover arbitrary surfaces and can detect the center of load distribution applied to 2-D surfaces as well as the total load. The wirings of numerous detection elements are connected only to adjacent elements such that there are only four output signal lines from the sensor. Further, the sensor, regardless of the number of elements, placement, and sensor area, the speeds of response were practically constant (within 1 ms). In this study, the sensor principle was explained and the prototypes were made. The basic characteristics defining the sensors were shown in the experiment results on position detection, load detection, and response characteristics.

Acknowledgment

We wish to express our thanks to Inaba Rubber Company, Ltd., for providing us with the prototype of the detector element. We wish to thank Dr. Carson Reynolds for valuable advice.

References

[1] H. R. Nicholls and M. H. Lee, "A survey of robot tactile sensing technology," *Int. J. Robotics Res.*, vol. 8, no. 3, pp. 3–30, 1989.
[2] M. H. Lee and H. R. Nicholls, "Tactile sensing for mechatronics—A state of the art survey," *Mechatronics*, vol. 9, pp. 1–31, 1999.
[3] V. J. Lumelsky, M. S. Shur, and S. Wagner, "Sensitive skin," *IEEE Sensors J.*, vol. 1, no. 1, pp. 41–51, Jan. 2001.
[4] H. Iwata and S. Sugano, "Whole-body covering tactile interface for human robot coordination," in *Proc. IEEE Int. Conf. Robot. Autom.*, 2002, vol. 4, pp. 3818–3824.
[5] T. Mukai, M. Onishi, T. Odashima, S. Hirano, and Z. Luo, "Development of the tactile sensor system of a human-interactive robot "RI-MAN"," *IEEE Trans. Robotics*, vol. 24, no. 2, pp. 505–512, Apr. 2008.
[6] M. Shimojo, A. Namiki, M. Ishikawa, R. Makino, and K. Mabuchi, "A tactile sensor sheet using pressure conductive rubber with electrical-wires stitched method," *IEEE Sensors J.*, vol. 5, no. 4, pp. 589–596, 2004.
[7] M. Inaba, Y. Hoshino, K. Nagasaka, T. Ninomiya, S. Kagami, and H. Inoue, "A full-body tactile sensor suit using electrically conductive fabric and strings," in *Proc. IEEE/RSJ Int. Conf. Intell. Robot. Syst.*, 1996, pp. 450–457.
[8] K. Seki, M. Shimojo, S. Sato, and A. Takahashi, "Development of a grasping pressure distribution sensor with high flexibility," *Trans. SICE*, vol. 31, no. 9, pp. 1528–1530, 1995.
[9] TekscanInc. [Online]. Available: http://www.tekscan.com/
[10] A. Nagakubo, H. Alirezaei, and Y. Kuniyoshi, "A tactile distribution sensor based on inverse problem theory," *J. Robot. Soc. Jpn.*, vol. 25, no. 6, pp. 162–171, 2007.
[11] Y. Ohmura, Y. Kuniyoshi, and A. Nagakubo, "Conformable and scalable tactile sensor skin for curved surfaces," in *Proc. IEEE Int. Conf. Robot. Autom.*, 2006, pp. 1348–1353.
[12] Y. Yamada, K. Yamamoto, N. Tsuchida, and M. Komai, "A transmission system for multiplex sensor signals using spread spectrum systems with synchronization tracking method," *J. Robot. Soc. Jpn.*, vol. 7, no. 1, pp. 11–18, 1989.
[13] M. Nilsson, "Tactile sensors and other distributed sensors with minimal wiring complexity," *IEEE/ASME Trans. Mechatronics*, vol. 5, no. 3, pp. 253–257, Sep. 2000.
[14] M. Hakozaki, H. Oasa, and H. Shinoda, "Telemetric robot skin," in *Proc. IEEE Int. Conf. Robot. Autom.*, 1992, vol. 2, pp. 957–961.

[15] H. Kawaguchi, T. Someya, T. Sekitani, and T. Sakurai, "Cut-and-paste customization of organic FET integrated circuit and its application to electronic artificial skin," *IEEE J. Solid-State Circuits*, vol. 40, no. 1, pp. 177–185, Jan. 2005.
[16] M. Shimojo, T. Araki, A. Ming, and M. Ishikawa, "A ZMP sensor for a biped robot," in *Proc. IEEE Int. Conf. Robot. Autom.*, 2005, pp. 1200–1205.
[17] M. Shimojo, T. Araki, S. Teshigawara, A. Ming, and M. Ishikawa, "A net-structure tactile sensor covering arbitrary surface and ensuring high-speed response," in *Proc. IEEE/RSJ Int. Conf. Intell. Robot. Syst.*, 2007, pp. 670–675.
[18] , A. L. Bovik, Ed., *Handbook of Image and Video Processing*, 2nd ed. New York: Elsevier, 2005, pp. 543–545.
[19] M. Shimojo, "Mechanical filtering effect of elastic cover for tactile sensor," *IEEE Trans. Robot. Autom.*, vol. 13, no. 1, pp. 128–132, Feb. 1997.

Makoto Shimojo received the B.E. degree in mechanical engineering from the University of Electro-Communications, Tokyo, Japan, in 1973, the M.E. Eng. degree from the Tokyo Institute of Technology, Tokyo, in 1976, and the Dr. Eng. degree from the University of Electro-Communications in 1993.

From 1976 to 1992, he was a Senior Researcher at Industrial Products Research Institute, Tsukuba, Japan. From 1993 to 1997, he was a Senior Researcher at the National Institute of Bioscience and Human Technology, Tsukuba. From 1985 to 1986, he was a Visiting Scholar at Stanford University, Stanford, CA. From 1997 to 2001, he was a Professor of Computer and Information Sciences at Ibaraki University. Since April 2001, he has been a Professor of Mechanical Engineering and Intelligent Systems at the University of Electro-Communications. His current research interests include mechatronics, tactile sensing system, and human interface using tactile information.

Prof. Shimojo is a Fellow of the Japan Society of Mechanical Engineers.

Takuma Araki is with Department of Mechanical Engineering and Intelligent Systems, University of Electro-Communications, Tokyo, Japan.

Aiguo Ming (M'02) received the B.E. degree in mechanical engineering from Hunan University, Hunan, China, in 1983, the M.E. degree in precision engineering from Yamanashi University, Yamanashi, Japan, in 1987, and the Dr. Eng. degree in precision engineering from the University of Tokyo, Tokyo, in 1990.

From 1990 to 1991, he was with Mitutoyo Corporation, Tokyo. From 1991 to 1994, he was a Research Associate with the Department of Mechanical Systems, Yamanashi University. Since 1994, he has been an Assistant Professor and then Associate Professor with the Department of Mechanical Engineering and Intelligent Systems, University of Electro-Communications. His current research interests include robotics and development of mechatronic systems.

Masatoshi Ishikawa received the B.E., M.E., and Dr. Eng. degrees in mathematical engineering and information physics from the University of Tokyo, Tokyo, Japan, in 1977, 1979, and 1988, respectively.

From 1979 to 1989, he was a Senior Researcher at the Industrial Products Research Institute, Tsukuba, Japan. From 1989 to 1999, he was an Associate Professor with the Department of Mathematical Engineering and Information Physics, University of Tokyo, where, from 1999 to 2001, he was a Professor. Since 2001, he has been a Professor of Information Physics and Computing at the University of Tokyo. His current research interests include parallel processing, smart sensor, vision chip, sensor fusion, robotics, and optical computing.